Stable Galerkin reduced order models for linearized compressible flow

Matthew F. Barone [a,*], Irina Kalashnikova [d,e], Daniel J. Segalman [b], Heidi K. Thornquist [c]

[a] *Wind Energy Technology Department, Sandia National Laboratories, P.O. Box 5800, MS 1124, Albuquerque, NM 87185-1124, United States*
[b] *Strategic Initiatives Department, Sandia National Laboratories, P.O. Box 5800, MS 0557, Albuquerque, NM 87185-0557, United States*
[c] *Electrical and Microsystem Modeling Department, Sandia National Laboratories, P.O. Box 5800, MS 0316, Albuquerque, NM 87185-0316, United States*
[d] *Aerosciences Department, Sandia National Laboratories, P.O. Box 5800, MS 0825, Albuquerque, NM 87185-0825, United States*
[e] *Institute for Computational and Mathematical Engineering, Stanford University, Stanford, CA 94305, United States*

ARTICLE INFO

ABSTRACT

The Galerkin projection procedure for construction of reduced order models of compressible flow is examined as an alternative discretization of the governing differential equations. The numerical stability of Galerkin models is shown to depend on the choice of inner product for the projection. For the linearized Euler equations, a symmetry transformation leads to a stable formulation for the inner product. Boundary conditions for compressible flow that preserve stability of the reduced order model are constructed. Preservation of stability for the discrete implementation of the Galerkin projection is made possible using a piecewise-smooth finite element basis. Stability of the reduced order model using this approach is demonstrated on several model problems, where a suitable approximation basis is generated using proper orthogonal decomposition of a transient computational fluid dynamics simulation.

1. Introduction

Simulation of time-varying, three-dimensional fluid flow remains and will continue to remain for some time, an expensive endeavor. This reality has motivated efforts to seek reduced order models (ROMs) that capture the essential dynamics of the full simulations, but at a much lower computational cost. Many ROM techniques in fluid mechanics are derived from the proper orthogonal decomposition (POD)/Galerkin projection approach [1–3]. The original intent of this approach was to develop low-dimensional models, containing only a few degrees of freedom, to enable and enhance understanding of the nonlinear dynamics of turbulent flows. Since then, other approaches to building ROMs have been proposed, each with its own inherent strengths, including the reduced basis method [4], balanced truncation [5,6] and goal-oriented ROMs [7]. The potential usefulness of ROMs has also since expanded to include predictive applications; for example, ROMs have been used in flow controller design [8], shape optimization [9] and aeroelastic stability analysis [10,11].

The use of POD/Galerkin ROMs in a predictive setting raises some fundamental questions regarding their numerical properties. In this setting the ROM may be viewed as an alternative discretization of the governing partial differential equations. As such, the essential properties of any such discretization are stability, consistency and convergence. In many situations satisfaction of the first two properties guarantees convergence. General results for any of the three properties are lacking for POD/Galerkin models of compressible fluid flow. This leads to practical limitations; for example, a ROM might be stable for a given number of modes, but unstable for other choices of basis size (see an example of this for a POD model in Bui-Thanh et al. [7]).

* Corresponding author. Tel.: +1 505 284 8686; fax: +1 505 844 6541.
  E-mail address: mbarone@sandia.gov (M.F. Barone).

The present work primarily addresses numerical stability of linear ROMs for compressible flow. The questions of consistency and convergence are not addressed. A POD basis, or any other empirical basis, is not usually complete, which complicates a general consistency analysis. Also not addressed is the related question of the behavior of a ROM when applied to a parameter space region not included in the ROM construction. There are promising developments in this area which can be applied; see, for example, Lieu and Farhat [12]. Despite the lack of a comprehensive numerical theory, it is still desirable to be able to generate a stable ROM regardless of the quality of the POD basis used to generate it. This is analogous to being able to run computational fluid dynamics simulations on a series of meshes, from coarse to fine and having confidence that the simulations will remain stable regardless of the mesh spacing.

Stable formulations for reduced order models have been proposed in other settings. Stability of reduced order models for electrical circuit analysis is considered by Freund and co-workers [13]. Preservation of the passivity, or energy dissipation, of the circuit system guarantees stability of the reduced order model. In fluid dynamics, Kwasniok [14] recognizes the role of energy conservation in ROMs of nonlinear, incompressible fluid flow for atmospheric modeling applications. The Galerkin projection approach is constructed so that the nonlinear terms in the ROM conserve turbulent kinetic energy or turbulent enstrophy.

These works and others demonstrate the importance of maintaining the proper energy balance in a reduced order model. Mathematically, the energy is expressed as an inner product, so that the stability of a reduced order model is often tied to the definition of this inner product. Rowley [6] has shown how balanced truncation may be viewed as a particular form of the POD, using the observability Gramian as an inner product. Balanced truncation and balanced POD methods are guaranteed to be stable for linear systems and also preserve the stability of an equilibrium point at the origin for nonlinear systems.

In the present work, we again demonstrate that the inner product used to define the Galerkin projection is closely tied to the stability of the resulting model. We further show how it is possible to construct stable ROMs for *any* choice of basis using Galerkin projection. An energy stability analysis is carried out for Galerkin methods applied to the linearized Euler equations, resulting in an inner product that guarantees certain stability bounds satisfied by the ROM. A means of implementing boundary conditions for the ROM that preserve stability is also developed. Implementation of the ROM is then defined in terms of finite element representations of the simulation data and of the POD modes. Along with numerical quadrature rules of sufficient accuracy, this approach ensures that the continuous stability estimates are satisfied by the discrete computer implementation. ROMs are then constructed for several model fluid flows using the schemes developed from the stability analysis.

2. The POD/Galerkin approach

This section describes the POD/Galerkin method for reducing the order of computational models for solving partial differential equations. The approach consists of two steps: calculation of a basis using the POD of an ensemble of flowfield realizations, followed by Galerkin projection of the governing partial differential equations onto the basis. The first step involves the transfer of kinematic information from the high-fidelity simulation to a relatively small number of modes. The second step involves a translation of the full-system dynamics to the implied dynamics of these modes. When successful, the result of this procedure is a set of time-dependent ordinary differential equations in the modal amplitudes that approximately describes the flow dynamics of the full-system of PDEs for some limited set of flow conditions.

2.1. Proper orthogonal decomposition

The proper orthogonal decomposition (POD) is a mathematical procedure that, given an ensemble of data, constructs a basis for the ensemble that is optimal in a well-defined sense. The mathematical development of POD for fluid flow applications in particular is described in detail in Lumley [15] and Holmes et al. [3]. The essentials of this development and the properties of POD most important to reduced order modeling are presented in this section.

Consider an ensemble $\{\mathbf{u}^k(\mathbf{x})\}$ of real vector fields on the domain $\mathbf{x} \in \Omega$. In the present context, the ensemble consists of a set of instantaneous snapshots of a numerical simulation solution field. The $\mathbf{u}$'s are assumed to belong to a Hilbert space $\mathcal{H}(\Omega)$ with associated inner product $(\mathbf{f}, \mathbf{g})$. Following the approach of Rowley et al. [16], we will defer the definition of the inner product until a particular application of the POD is considered, requiring only that it obey the usual requirements for an inner product. Note that this results in a general formulation for the POD that differs in some aspects from formulas derived for the $L^2(\Omega)$ Hilbert space.

The POD basis is a set of functions $\{\phi_j(\mathbf{x})\}$ that is the "best" linear basis for description of the ensemble. The flowfield state vector $\mathbf{u} \in \text{span}\{\phi_j\}$ is represented as a linear combination of the POD modes,

$$\mathbf{u}(\mathbf{x}, t) = \sum_j a_j(t)\phi_j(\mathbf{x}). \tag{1}$$

The POD modes, or empirical eigenfunctions, are defined by requiring that the averaged projection of the ensemble $\mathbf{u}^k$ onto ϕ is a maximum:

$$\max_{\phi \in \mathcal{H}(\Omega)} \frac{\langle (\mathbf{u}, \phi)^2 \rangle}{\|\phi\|^2}, \tag{2}$$

where $\|\cdot\|$ is the norm generated by the inner product. The averaging operator $\langle\cdot\rangle$ used in (2) could be an ensemble average over many separate flow realizations, or it could be a time-average taken from different samples of a single realization.

The constrained optimization problem (2) with constraint $\|\phi\| = 1$ reduces to the eigenvalue problem

$$\mathbf{R}\phi = \lambda\phi, \tag{3}$$

where

$$\mathbf{R}\phi \equiv \langle\mathbf{u}^k(\mathbf{u}^k, \phi)\rangle. \tag{4}$$

The operator $\mathbf{R}$ is self-adjoint and non-negative definite; if we further assume that $\mathbf{R}$ is compact, then there are exists a countable set of non-negative eigenvalues λ_i, with associated eigenfunctions ϕ_i. The eigenfunctions, appropriately normalized, form an orthonormal subspace of $\mathcal{H}$, i.e. $(\phi_i, \phi_j) = \delta_{ij}$.

The POD modes are the eigenfunctions ϕ_i associated with nonzero λ_i. Taking the inner product of (3) with ϕ, it is straightforward to show that $\langle(\mathbf{u}^k, \phi_i)^2\rangle = \lambda_i$. In other words, the magnitude of the eigenvalue is equivalent to the average energy of the projection of the ensemble onto the associated eigenfunction, where the square of the projection is interpreted as an energy measure. The POD modes may be ordered according to the magnitude of their eigenvalue, with λ_1, ϕ_1 equal to the eigenvalue/eigenfunction pair with the largest eigenvalue, λ_N equal to the smallest non-zero eigenvalue and $\lambda_1 > \lambda_2 > \cdots > \lambda_n > \cdots > \lambda_N$. In building reduced order models one is interested in truncating the POD basis and retaining only the $M < N$ most energetic modes. It can be shown that the sequence of truncated POD bases forms an optimal set, in the sense that a POD basis comprised of M modes describes more energy (on average) of the ensemble than any other *linear* basis of the same dimension M. This compression of the ensemble energy into a minimum number of modes makes the POD basis attractive for reduced order modeling.

In practice, the $\mathbf{u}^k$ are vectors of state variables at discrete grid point locations, each containing a single solution from the numerical simulation. They will have length Nr, where N is the total number of grid points and r is the number of dependent variables describing the flow state. Thus, the discretized version of (3) will be an eigenvalue problem of order Nr. For $N \gg K$, where K is the number of flowfield snapshots used, this procedure is costly and, it turns out, inefficient. Sirovich [17] showed how the eigenvalue problem (3) can be reduced to order K, resulting in a much more efficient procedure for $N \gg K$. This is the so-called "method of snapshots" for computing a POD basis.

2.2. Galerkin projection

The second step for constructing the reduced order model is to project the governing PDEs onto the POD basis.

Consider a generic nonlinear PDE, containing a linear term as well as quadratic and cubic nonlinearities, that governs the behavior of a time-dependent vector field $\mathbf{u}(\mathbf{x}, t)$,

$$\frac{\partial\mathbf{u}}{\partial t} = \mathcal{L}\mathbf{u} + \mathcal{N}_2(\mathbf{u}, \mathbf{u}) + \mathcal{N}_3(\mathbf{u}, \mathbf{u}, \mathbf{u}). \tag{5}$$

The operator $\mathcal{L}$ is a linear operator, $\mathcal{N}_2$ is a quadratic nonlinear operator and $\mathcal{N}_3$ is a cubic nonlinear operator. The Galerkin projection of Eq. (5) onto each POD mode ϕ_j is

$$\left(\frac{\partial\mathbf{u}}{\partial t}, \phi_j\right) = (\mathcal{L}\mathbf{u}, \phi_j) + (\mathcal{N}_2(\mathbf{u}, \mathbf{u}), \phi_j) + (\mathcal{N}_3(\mathbf{u}, \mathbf{u}, \mathbf{u}), \phi_j). \tag{6}$$

Substituting the POD decomposition for $\mathbf{u}$ into (6), applying the algebraic rules of inner products along with orthogonality of the POD basis gives

$$\frac{\mathrm{d}a_k}{\mathrm{d}t} = \sum_l a_l(\phi_k, \mathcal{L}(\phi_l)) + \sum_{l,m} a_l a_m(\phi_k, \mathcal{N}_2(\phi_l, \phi_m)) + \sum_{l,m,n} a_l a_m a_n(\phi_k, \mathcal{N}_3(\phi_l, \phi_m, \phi_n)). \tag{7}$$

This is the reduced order model for Eq. (5) by the POD/Galerkin method. It is a time-dependent system of ODE's of order equal to the number of retained POD modes M, with $k = 1, 2, \ldots, M$. The inner products in (7) are functionals of the known, time-independent POD modes $\phi(\mathbf{x})$, and may be precomputed before integration of the ROM.

The Galerkin projection step here is applied to the original, continuous PDEs. In many applications of reduced order modeling, the discrete representation of the equations is projected onto the modes. This discrete approach has the advantage that, depending on the implementation, boundary condition terms present in the discretized equation set are inherited by the ROM. Also, certain properties of the numerical scheme used to solve the full equations may be inherited by the ROM. The continuous approach, used in the present work, has the advantages that is does not require an intrusive or code-specific implementation and it may be more amenable to analysis.

2.3. Inner product

The inner product serves several purposes in the POD/Galerkin procedure. Fundamentally, it helps define the Hilbert space on which the analysis proceeds. It defines the projection of a solution onto the POD basis, and thereby also defines

the mathematical quantity that the POD basis optimally represents. It also defines the projection of the governing equations onto the POD basis, which leads to the POD/Galerkin dynamical model.

The majority of POD/Galerkin models for fluid flow have used the incompressible Navier–Stokes equations as the governing equation set. In this case, a natural choice of inner product is the L^2 inner product, defined here on the spatial domain Ω,

$$(u, v) = \int_\Omega u v \, \mathrm{d}\Omega. \tag{8}$$

This is because if the solution vector is taken to be the velocity vector u_i, then the inner product corresponds to a measure of the global kinetic energy. This makes the POD basis physically sensible, since the modes optimally represent the kinetic energy present in the ensemble from which they are generated. This choice also leads to a straightforward representation of the solution energy in terms of modal amplitudes. Suppose an orthonormal set of POD modes is used to represent the velocity field,

$$u_i = \sum_{k=1}^{M} a_k(t) \phi_k^i(\mathbf{x}), \tag{9}$$

then the global kinetic energy at any instant in time is

$$2E = (u_i, u_i) = \sum_{k=1}^{M} a_k^2. \tag{10}$$

3. Stability of Galerkin approximations

This section examines stability of Galerkin approximations to a class of linear partial differential equations, as well as stability of such approximations to equations governing linearized compressible flow. In the initial theoretical development, C^∞ smooth solutions and equation coefficients are assumed. The smoothness assumption will be relaxed when the discrete computer implementation of the method is discussed. The stability properties of the PDEs are established first using the energy method. A stable Galerkin projection scheme is then derived based on the results of the energy method analysis.

3.1. Stability for a scalar linear equation

Consider the scalar initial value problem, or Cauchy problem,

$$\frac{\partial u}{\partial t} = Lu, \quad x \in \mathbf{R}^n, \quad t \geqslant 0, \tag{11}$$
$$u(x, 0) = f(x). \tag{12}$$

Here L is a linear differential operator with constant coefficients. The operator L is *semi-bounded* w.r.t. the inner product $(\cdot, \cdot)_E$ if it satisfies the following inequality for all sufficiently smooth functions $w = w(x)$, $w \in L^2$,

$$(w, Lw)_E \leqslant \alpha(w, w)_E, \tag{13}$$

where α is a real constant. In this case, well-posedness follows from the relation

$$\frac{\mathrm{d}}{\mathrm{d}t}(u, u)_E \leqslant \alpha(u, u)_E. \tag{14}$$

In fact, the following theorem holds [18]:

The Cauchy problem given by (11) is well-posed if and only if the operator L is semibounded w.r.t. an inner product $(\cdot, \cdot)_E$ which corresponds to a norm equivalent to the L_2-norm.

Now consider a Galerkin approximation to (11), $u_N \in \mathcal{H}$, satisfying

$$\left(\frac{\partial u_N}{\partial t}, \phi \right)_E = (Lu_N, \phi)_E \tag{15}$$

for all $\phi \in \mathcal{H}$ and suppose that L is semi-bounded w.r.t. $(\cdot, \cdot)_E$. Setting $\phi = u_N$ leads to the following stability estimate for the Galerkin approximation [19,20]:

$$\frac{1}{2} \frac{\mathrm{d}}{\mathrm{d}t} \|u_N\|_E^2 \leqslant \alpha \|u_N\|_E^2. \tag{16}$$

Thus,

$$\|u_N(x, t)\|_E \leqslant e^{\alpha t} \|u_N(x, 0)\|_E. \tag{17}$$

The result (17) means that the numerical solution is bounded in a way consistent with behavior of exact solutions of the original differential equation, i.e. it is stable. The practical implication of these results is the opportunity to pose a stable

Galerkin approximation to a well-posed linear differential equation by choosing an appropriate inner product, one with respect to which the differential operator is semi-bounded. These results can be extended to variable-coefficient operators, including linear hyperbolic systems of equations such as the linearized Euler equations (discussed in the next section).

3.2. Stability of the Galerkin approximation for compressible flow

3.2.1. Stability for a linear hyperbolic system of equations

This section, based on the energy method analysis of Gustafsson and Sundstrom [21], extends the stability result obtained previously for scalar equations to symmetrizable hyperbolic systems of equations.

First consider a linear hyperbolic system of equations for $x \in R^n$

$$\frac{\partial u}{\partial t} + A_j \frac{\partial u}{\partial x_j} + Cu = 0 \tag{18}$$

In this notation u is a $r \times 1$ vector and A_j and C are $r \times r$ matrices that vary smoothly in space but do not vary with time. Suppose that this equation can be symmetrized by introduction of a positive definite symmetric $r \times r$ matrix H,

$$H \frac{\partial u}{\partial t} + HA_j \frac{\partial u}{\partial x_j} + HCu = 0 \tag{19}$$

such that HA_j are each symmetric matrices. Then, using the symmetry properties of H and HA_j, the following energy expression is derived:

$$\frac{\partial}{\partial t} \int_\Omega u^T H u \, d\Omega = - \int_{\partial\Omega} u^T H(A_j n_j) u \, dS + \int_\Omega u^T \left(\frac{\partial}{\partial x_j}(HA_j) - HC - C^T H \right) u \, d\Omega. \tag{20}$$

Now consider the pure initial value problem, ignoring the contribution from the boundary surface integral in (20). Noting that H can be decomposed into $H = Q^T Q$, the right hand side of (20) is

$$\int_\Omega u^T \left(\frac{\partial}{\partial x_j}(HA_j) - HC - C^T H \right) u \, d\Omega = \int_\Omega u^T Q^T \left(Q^{T^{-1}} \frac{\partial}{\partial x_j}(HA_j)Q^{-1} - QCQ^{-1} - (QCQ^{-1})^T \right) Qu \, d\Omega. \tag{21}$$

Thus (20) becomes

$$\frac{\partial}{\partial t} \int_\Omega u^T H u \, d\Omega \leqslant 2\alpha \int_\Omega u^T H u \, d\Omega, \tag{22}$$

where 2α is an upper bound on the eigenvalues of

$$Q^{T^{-1}} \frac{\partial}{\partial x_j}(HA_j)Q^{-1} - QCQ^{-1} - (QCQ^{-1})^T.$$

The integral $(u, v)_H \equiv \int_\Omega u^T H v \, d\Omega$ is an energy inner product. The corresponding energy norm $\|u\|_H = (u, u)_H^{1/2}$ is equivalent to the L^2 norm and establishes well-posedness (recall Section 3.1) by satisfying

$$\|u(x, t)\|_H \leqslant e^{\alpha t} \|u(x, 0)\|_H. \tag{23}$$

In turn, the corresponding Galerkin approximation u_N using the energy norm satisfies the stability condition

$$\|u_N(x, t)\|_H \leqslant e^{\alpha t} \|u_N(x, 0)\|_H. \tag{24}$$

3.2.2. Stability for the linearized Euler equations

If a compressible fluid system can be described by inviscid, small-amplitude perturbations about a steady-state mean flow, then the linearized Euler equations may be used. In the following development, stability estimates for the linearized Euler equation initial value problem are derived, which lead to stable Galerkin approximations using appropriate inner products. The stability results follow from the results of the previous section, since the linearized Euler equations are a symmetrizable hyperbolic system of PDEs. Note that many other hyperbolic systems of interest are symmetrizable, particularly those that are derived from conservation laws. Examples include the nonlinear Euler equations, compressible Navier–Stokes equations [22] and the shallow water equations [23]. It is possible to derive the symmetrizer of a matrix, or set of matrices, using the eigenvectors of the matrix (or matrices); see, e.g. Ref. [24].

For the compressible fluid, let the state vector be decomposed into a steady mean and time-varying fluctuating part, $\mathbf{q}(\mathbf{x}, t) = \bar{\mathbf{q}}(\mathbf{x}) + \mathbf{q}'(\mathbf{x}, t)$, where $\mathbf{q} = [u \quad v \quad w \quad \zeta \quad p]^T$. The three components of the velocity vector are u, v and w, the specific volume is ζ and the pressure is p. The density ρ is the inverse of the specific volume. The linearized Euler equations in these variables are:

$$\frac{\partial \mathbf{q}'}{\partial t} + \mathbf{A}(\bar{\mathbf{q}}) \cdot \nabla \mathbf{q}' + C(\bar{\mathbf{q}})\mathbf{q}' = 0 \tag{25}$$

where

$$\mathbf{A}(\bar{\mathbf{q}}) \equiv [A_x(\bar{\mathbf{q}}), A_y(\bar{\mathbf{q}}), A_z(\bar{\mathbf{q}})]^T,$$

$$A_x = \begin{bmatrix} \bar{u} & 0 & 0 & 0 & \bar{\zeta} \\ 0 & \bar{u} & 0 & 0 & 0 \\ 0 & 0 & \bar{u} & 0 & 0 \\ -\bar{\zeta} & 0 & 0 & \bar{u} & 0 \\ \gamma\bar{p} & 0 & 0 & 0 & \bar{u} \end{bmatrix} \quad A_y = \begin{bmatrix} \bar{v} & 0 & 0 & 0 & 0 \\ 0 & \bar{v} & 0 & 0 & \bar{\zeta} \\ 0 & 0 & \bar{v} & 0 & 0 \\ 0 & -\bar{\zeta} & 0 & \bar{v} & 0 \\ 0 & \gamma\bar{p} & 0 & 0 & \bar{v} \end{bmatrix} \quad A_z = \begin{bmatrix} \bar{w} & 0 & 0 & 0 & 0 \\ 0 & \bar{w} & 0 & 0 & 0 \\ 0 & 0 & \bar{w} & 0 & \bar{\zeta} \\ 0 & 0 & -\bar{\zeta} & \bar{w} & 0 \\ 0 & 0 & \gamma\bar{p} & 0 & \bar{w} \end{bmatrix}$$

$$C = \begin{bmatrix} \frac{\partial \bar{u}}{\partial x} & \frac{\partial \bar{u}}{\partial y} & \frac{\partial \bar{u}}{\partial z} & \frac{\partial \bar{p}}{\partial x} & 0 \\ \frac{\partial \bar{v}}{\partial x} & \frac{\partial \bar{v}}{\partial y} & \frac{\partial \bar{v}}{\partial z} & \frac{\partial \bar{p}}{\partial y} & 0 \\ \frac{\partial \bar{w}}{\partial x} & \frac{\partial \bar{w}}{\partial y} & \frac{\partial \bar{w}}{\partial z} & \frac{\partial \bar{p}}{\partial z} & 0 \\ \frac{\partial \bar{\zeta}}{\partial x} & \frac{\partial \bar{\zeta}}{\partial y} & \frac{\partial \bar{\zeta}}{\partial z} & -\left(\frac{\partial \bar{u}}{\partial x} + \frac{\partial \bar{v}}{\partial y} + \frac{\partial \bar{w}}{\partial z}\right) & 0 \\ \frac{\partial \bar{p}}{\partial x} & \frac{\partial \bar{p}}{\partial y} & \frac{\partial \bar{p}}{\partial z} & 0 & \gamma\left(\frac{\partial \bar{u}}{\partial x} + \frac{\partial \bar{v}}{\partial y} + \frac{\partial \bar{w}}{\partial z}\right) \end{bmatrix}$$

In this case, the symmetrizing matrix H is given by

$$H = \begin{bmatrix} \bar{\rho} & 0 & 0 & 0 & 0 \\ 0 & \bar{\rho} & 0 & 0 & 0 \\ 0 & 0 & \bar{\rho} & 0 & 0 \\ 0 & 0 & 0 & \alpha^2\gamma\bar{\rho}^2\bar{p} & \bar{\rho}\alpha^2 \\ 0 & 0 & 0 & \bar{\rho}\alpha^2 & \frac{(1+\alpha^2)}{\gamma\bar{p}} \end{bmatrix} \tag{26}$$

where α^2 is an arbitrary real, nonzero parameter. The "symmetry inner product" is then[1]

$$(\mathbf{q}'^{(1)}, \mathbf{q}'^{(2)})_H = \int_\Omega \left[\bar{\rho}(u'^{(1)} u'^{(2)} + v'^{(1)} v'^{(2)} + w'^{(1)} w'^{(2)}) + \alpha^2\gamma\bar{\rho}^2\bar{p}\zeta'^{(1)}\zeta'^{(2)} + \frac{1+\alpha^2}{\gamma\bar{p}}p'^{(1)}p'^{(2)} + \alpha^2\bar{\rho}\left(\zeta'^{(2)}p'^{(1)} + \zeta'^{(1)}p'^{(2)}\right) \right] d\Omega. \tag{27}$$

Due to the result for linear hyperbolic systems given by Eq. (24), Galerkin approximations for the linearized Euler equations based on the inner product $(\cdot,\cdot)_H$ are stable (for the initial value problem). Introducing a modal basis $\mathbf{q}'_M = \sum_{k=1}^M a_k(t)\boldsymbol{\phi}_k(\mathbf{x})$ with

$$\boldsymbol{\phi}_j = \begin{bmatrix} \phi_j^1 & \phi_j^2 & \phi_j^3 & \phi_j^4 & \phi_j^5 \end{bmatrix}^T, \tag{28}$$

the Galerkin projection is

$$\left(\boldsymbol{\phi}_j, \frac{\partial \mathbf{q}'_M}{\partial t}\right)_H + (\boldsymbol{\phi}_j, \mathbf{A}(\bar{\mathbf{q}}) \cdot \nabla \mathbf{q}'_M)_H + (\boldsymbol{\phi}_j, C(\bar{\mathbf{q}})\mathbf{q}'_M)_H = 0. \tag{29}$$

Substituting the modal basis into (29) leads to the ROM,

$$\dot{a}_j = -\sum_{k=1}^M a_k(\boldsymbol{\phi}_j, \mathbf{A}(\bar{\mathbf{q}}) \cdot \nabla\boldsymbol{\phi}_k)_H - \sum_{k=1}^M a_k(\boldsymbol{\phi}_j, C(\bar{\mathbf{q}})\boldsymbol{\phi}_k)_H. \tag{30}$$

Note that for a spatially uniform mean state, the result from Eq. (22) applied to the linearized Euler equations leads to

$$\frac{\partial}{\partial t} \int_\Omega \mathbf{q}'^T H \mathbf{q}' \, d\Omega = 0, \tag{31}$$

and the semi-discrete Galerkin approximation satisfies the strong stability condition

$$\|\mathbf{q}'_M(t)\|_H = \|\mathbf{q}'_M(0)\|_H. \tag{32}$$

The uniform mean flow case allows for a clean stability analysis, since the mean flow supports only neutral or decaying disturbances. For non-uniform flow the continuous equations may support exponentially growing instabilities, an example of which is the Kelvin–Helmholtz shear layer instability. It is then difficult to distinguish between natural instability modes supported by the continuous equations and spurious instabilities generated by the numerical discretization.

Note that the symmetry inner product introduced here is only directly applicable to Galerkin approximations of the *linearized* Euler equations. One could consider adapting this inner product to a Galerkin treatment of the full nonlinear Euler

---

[1] This form of the symmetrization follows the derivation of Gustafsson and Sundstrom [21]. Other symmetric forms of both the linearized Euler and linearized Navier–Stokes equations can be found in Oliger and Sundstrom [25] and in Abarbanel and Gottlieb [26]. In an earlier work, Chu [27] derived a disturbance energy equation using a similar inner product without explicit consideration of symmetrization.

equations by specifying a steady mean flow and projecting the resulting quasi-linear equations using the symmetry inner product. This would not necessarily lead to a stable approximation, since the fluctuations about the specified mean state will, in general, be nonlinear. However, in practice this may provide a superior inner product than other naïve choices, e.g. the L^2 inner product.

This situation differs from the usual stability arguments applied to finite difference/finite volume type discretizations of hyperbolic equations. There, the stability of the discretization for linearized "frozen coefficient" equations leads to stability of the method when applied to the corresponding nonlinear equations. This is due to the fact that implementation of these methods uses the same type of time-linearization as that of the stability analysis. For a POD/Galerkin method of the type considered here, this is not possible since both the POD computation and the projection depend upon a specified weighted inner product, the weights of which are not a function of time.

4. Fluid ROM boundary conditions

Boundary conditions may be efficiently implemented for a Galerkin ROM using a weak formulation. Further, the energy stability analysis of Section 3.2 allows for weak boundary conditions that preserve stability.

Consider Galerkin projection of the linearized Euler equations onto a modal basis $\{\phi_j\}$. Also assume a uniform base flow, such that $\nabla \bar{\mathbf{q}} = 0$. Integrating the second term of (29) by parts gives

$$\left(\phi_j, \frac{\partial \mathbf{q}'_M}{\partial t}\right)_H = -\int_{\partial \Omega} \phi_j^T H(\bar{\mathbf{q}})(\mathbf{A}(\bar{\mathbf{q}}) \cdot \mathbf{n}) \mathbf{q}'_M \, dS + \int_{\Omega} (\nabla \cdot [\phi_j^T H(\bar{\mathbf{q}}) \mathbf{A}(\bar{\mathbf{q}})]) \mathbf{q}'_M \, d\Omega. \tag{33}$$

Boundary conditions may now be implemented through modification of the perturbed state by substituting $\mathbf{q}'_M \leftarrow \mathbf{q}'_b$ in the boundary integral appearing in (33).

Inviscid compressible flow boundary conditions are most often implemented in terms of local one-dimensional characteristics defined in the direction normal to the boundary. As detailed in the Appendix, the matrix $\mathbf{A}(\bar{\mathbf{q}}) \cdot \mathbf{n}$ may be diagonalized using the transformation

$$\mathbf{A}(\bar{\mathbf{q}}) \cdot \mathbf{n} = \mathbf{S} \mathbf{\Lambda} \mathbf{S}^{-1}, \tag{34}$$

where the vector of "characteristic variables" is defined as

$$\mathbf{V}' = \mathbf{S}^{-1} \mathbf{q}'. \tag{35}$$

The boundary conditions are then given on the domain boundary $\partial \Omega$ as $\mathbf{V}' = \mathbf{V}'_b$. The elements of the vector $\mathbf{V}'_b$ corresponding to outgoing characteristic waves are constructed from the local numerical solution, while elements corresponding to incoming characteristics are specified. Eq. (33) in terms of characteristic boundary conditions is

$$\left(\phi_j, \frac{\partial \mathbf{q}'_M}{\partial t}\right)_H = -\int_{\partial \Omega} \phi_j^T H(\bar{\mathbf{q}}) \mathbf{S} \mathbf{\Lambda} \mathbf{V}'_b \, dS + \int_{\Omega} (\nabla \cdot [\phi_j^T H(\bar{\mathbf{q}}) \mathbf{A}(\bar{\mathbf{q}})]) \mathbf{q}'_M \, d\Omega. \tag{36}$$

Stability of the boundary value problem is examined by substituting $\mathbf{q}'_M$ for ϕ in (36). Making this substitution, exploiting the symmetry of $H(\bar{\mathbf{q}})\mathbf{A}(\bar{\mathbf{q}})$ and integrating by parts once again gives

$$\frac{1}{2} \frac{d}{dt} \|\mathbf{q}'_M\|_H^2 = \int_{\partial \Omega} \left(\frac{1}{2} \mathbf{q}_M'^T H(\bar{\mathbf{q}})(\mathbf{A}(\bar{\mathbf{q}}) \cdot \mathbf{n}) \mathbf{q}'_M - \mathbf{q}_M'^T H(\bar{\mathbf{q}}) \mathbf{S} \mathbf{\Lambda} \mathbf{V}'_b\right) dS. \tag{37}$$

Stable boundary conditions are those for which the right hand side of (37) is non-positive.

Implementation of the boundary conditions is simplified if the ROM without boundary conditions is calculated first, according to (30). Denoting the unmodified boundary integral $I_{bu_{jk}} \equiv \int_{\partial \Omega} \phi_j^T H(\bar{\mathbf{q}})(\mathbf{A}(\bar{\mathbf{q}}) \cdot \mathbf{n}) \phi_k \, dS$ and the boundary integral with boundary conditions enforced as $I_{b_{jk}}$, the ROM becomes

$$\dot{a}_j = -\sum_{k=1}^{M} a_k (\phi_j, \mathbf{A}(\bar{\mathbf{q}}) \cdot \nabla \phi_k)_H - \sum_{k=1}^{M} a_k (\phi_j, C(\bar{\mathbf{q}}) \phi_k)_H + \sum_{k=1}^{M} a_k (I_{bu_{jk}} - I_{b_{jk}}). \tag{38}$$

4.1. Solid surface boundary condition

The linearized solid wall boundary condition for a surface with unit normal $\mathbf{n}$ (pointing out of the fluid domain), displaced a small distance η from equilibrium and moving at velocity $\dot{\eta}$ in the direction of $-\mathbf{n}$, is

$$\mathbf{u}' \cdot \mathbf{n} = -\dot{\eta} - \bar{\mathbf{u}} \cdot \nabla \eta \equiv u'_b. \tag{39}$$

Here $\mathbf{u} \equiv [u \ v \ w]^T$ is the fluid velocity vector. The solid wall boundary condition is posed as a perfectly reflecting condition, using the characteristic decomposition. For a stationary wall, the incoming characteristic, V'_5, is set equal to the outgoing characteristic, V'_4. When the wall velocity is u'_b, the following relation satisfies the boundary condition (39):

$$V'_5 = V'_4 - 2u'_b \tag{40}$$

The boundary integrand in (33) becomes

$$\boldsymbol{\phi}_j^T H(\bar{\mathbf{q}})(\mathbf{A}(\bar{\mathbf{q}}) \cdot \mathbf{n})\mathbf{q}_M' = \bar{\rho}\bar{c}\phi_j^n(\mathbf{u}_\mathbf{M}' \cdot \mathbf{n} - u_b') + \phi_j^n p_M' + \phi_j^5 u_b'. \tag{41}$$

where

$$\phi_j^n \equiv (n_1\phi_j^1 + n_2\phi_j^2 + n_3\phi_j^3). \tag{42}$$

The last two terms in the boundary integrand are the same as the unaltered integrand, only with $\mathbf{u}_\mathbf{M}' \cdot \mathbf{n} = u_b'$, while the first term acts as a penalty term that forces the velocity to the prescribed boundary value.

Evaluation of the stability relation (37), assuming $u_b' = 0$ gives

$$\frac{1}{2}\frac{\mathrm{d}}{\mathrm{d}t}\|\mathbf{q}_M'\|_H^2 = -\bar{\rho}\bar{c}(\mathbf{u}_M' \cdot \mathbf{n})^2 \leqslant 0, \tag{43}$$

showing that the boundary condition for the Galerkin scheme is stable, even when the approximation modes do not themselves satisfy the boundary condition.

Inserting the modal representation for p_M' and $\mathbf{u}_M'$ into (41) and applying the surface integral over the no-penetration surface $\partial\Omega_P$, leads to the following term appearing in the jth ROM equation:

$$I_{P_j} = \sum_{k=1}^{M} a_k(t) \int_{\partial\Omega_P} \phi_j^n(\phi_k^5 + \bar{\rho}\bar{c}\phi_k^n)\,\mathrm{d}S + \int_{\partial\Omega_P} (\phi_j^5 - \bar{\rho}\bar{c}\phi_j^n)u_b'\,\mathrm{d}S. \tag{44}$$

4.2. Far-field boundary conditions

Far-field conditions may be useful and, in some cases, necessary for stability of a ROM formulation. The computational fluid dynamics (CFD) code used to generate the fluid modal basis incorporates some form of farfield boundary condition which, if it is a linear boundary condition, will also be satisfied by the fluid modes due to the properties of POD. However, to ensure a well-posed and stable Galerkin approximation, farfield boundary conditions can be incorporated into the ROM.

Consider the boundary integral term from (33) evaluated over a farfield boundary $\partial\Omega_F$. The procedure for application of an approximately non-reflecting condition is as follows. The components of $\mathbf{V}'$ corresponding to characteristic waves traveling into the domain are set to zero. The terms in the boundary integrand are re-cast in terms of the modal representation, which leads to boundary terms in the ROM. It can be proven that, like the solid wall condition, this boundary condition formulation results in a stable Galerkin scheme for uniform flow. The details of the far-field boundary condition implementation are given in the Appendix.

5. Approximation space and numerical quadrature

Thus far, the stability estimates and associated inner products for Galerkin ROMs have only been given in continuous form. They are valid only if the relevant integrals are evaluated exactly. This is similar to the situation occurring in numerical analysis of spectral methods. With spectral methods, this problem is generally resolved by applying a high-precision numerical quadrature that is able to integrate exactly the spectral projections. We borrow from this approach in the following way. The POD basis is first described by a finite element representation on the computational mesh. This is fairly general, as long as the simulation code can output data to a nodal mesh and the mesh can be cast as a collection of finite elements. In the present work we use piecewise-linear (C^0) finite elements to represent the snapshot data and the POD modes. It is then possible to construct a numerical quadrature operator that exactly integrates the inner product of the finite element representations. The introduction of C^0 finite elements requires a relaxation of the smoothness requirements on $\mathbf{q}'$, $H(\bar{\mathbf{q}})$ and $\mathbf{A}(\bar{\mathbf{q}})$. The projection integrals are then to be interpreted in the sense of distributions.

Consider the d-dimensional spatial domain Ω, subdivided into N_e elements, $\Omega_e, e = 1, \ldots, N_e$. The finite element representation of the state variable $\mathbf{q}'$ is

$$\mathbf{q}_e'^h(\mathbf{x}) = \sum_{i=1}^{N_n} N_i(\mathbf{x})\mathbf{q}_i', \quad \mathbf{x} \in \Omega_e \tag{45}$$

where N_n is the number of nodes that define the element Ω_e and N_i are the linear shape functions. Consider the case of linear tetrahedral elements, where $N_n = 4$ and the shape functions span the space of all possible linear functions on the element. A quadratic function $f(\mathbf{x})$ can be integrated exactly over an element by a quadratic Gauss quadrature rule of the form

$$\int_\Omega f(\mathbf{x})\,\mathrm{d}\Omega_e = \sum_{j=1}^{4} \omega_{j_e}' f(\mathbf{x}_{j_e}), \tag{46}$$

where ω_{j_e}' are the integration weights and the $\mathbf{x}_{j_e}$ are the Gauss integration points of the element.

Now suppose the integral to be computed is a weighted inner product of two state vector realizations $\mathbf{u}(\mathbf{x})$ and $\mathbf{v}(\mathbf{x})$,

$$(\mathbf{u}, \mathbf{v})_H = \int_\Omega \mathbf{u}^T H(\bar{\mathbf{q}}) \mathbf{v} \, \mathrm{d}\Omega. \tag{47}$$

The discrete representations of the vectors $\mathbf{u}$ and $\mathbf{v}$ are written as $\mathbf{u}^h$ and $\mathbf{v}^h$, respectively, with length equal to the number of mesh nodes N times the dimension of the vector, r. Let $H_e^h(\bar{\mathbf{q}})$ be the $r \times r$ element inner product matrix, taken to be piecewise constant over each element. The formula for numerical integration can be written

$$(\mathbf{u}, \mathbf{v})_H = \mathbf{u}^{h^T} W \mathbf{v}^h \tag{48}$$

where W is a sparse block matrix comprised of $N \times N$ blocks of dimension $r \times r$. The k,lth block of W is $w_{kl}I$, with

$$w_{kl} = \sum_{e=1}^{N_{kl}^e} H_e^h \sum_{j=1}^4 N_{k_e}(\mathbf{x}_{j_e}) N_{l_e}(\mathbf{x}_{j_e}) \omega'_{j_e}, \tag{49}$$

and where the outer sum is over the elements connected to the k–l nodal "edge."

The finite element representation and associated Gauss quadratures allow for a general and flexible means of creating stable, projection-based ROMs. The only requirements are that data are stored at nodes of the mesh and that the mesh can be decomposed into finite elements of the desired order. Higher order representations of the base flow and inner product matrix $H(\bar{\mathbf{q}})$ are also possible, given a quadrature rule of sufficient order.

6. Results

The method for generating stable ROMs is exercised on several model problems in this section. Emphasis is placed on reproducing a given CFD solution for a single set of flow conditions in a stable and accurate fashion. This is viewed as an essential pre-requisite for applying the method to more complex situations, such as building ROMs valid across a parameter space or range of flow conditions.

6.1. ROM generation procedure

For the results presented in this section, the fluid simulation data were generated using the AERO-F simulation code [28]. AERO-F is an arbitrary Lagrangian–Eulerian code that can be used for high-fidelity aeroelastic analysis. The linearized Euler solver capability of AERO-F was used in the present work; details of the finite volume discretization and linearization can be found in Lieu et al. [11].

The fluid ROMs were built using nondimensionalized equations and CFD solutions. The nondimensionalization used was $\zeta^* = \zeta/\zeta_{ref}$, $u^* = u/c_{ref}$, $v^* = v/c_{ref}$, $w^* = w/c_{ref}$, $p^* = p/\rho_{ref} c_{ref}^2$, where * quantities are non-dimensional.
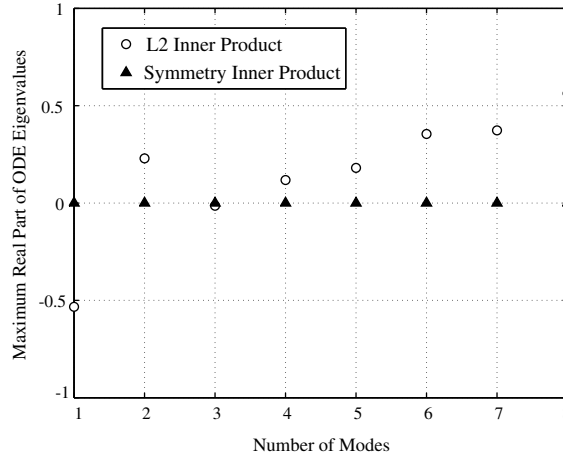
The fluid POD modes are generated by solution of an eigenproblem, as explained in Section 2. A code was written that reads in the snapshot data written by AERO-F, assembles the necessary finite element representation of the snapshots and computes the numerical quadrature necessary for evaluation of the inner products. The code performs all the calculations in parallel using distributed matrix and vector data structures and parallel eigensolvers from the Trilinos project [29], allowing for large data sets and a relatively large number of POD modes. The `libmesh` finite element library [30] was used to compute element quadratures. This code also projects the modes onto the linearized Euler equations and outputs the resulting fluid ROM coefficient matrix.

6.2. Test case: random basis

To demonstrate the stability properties of the fluid ROM, we first consider the case where the modal basis is composed of a sequence of random vector fields that decay to zero at the boundary. The spatial domain is a rectangular prism, discretized by tetrahedral elements. The base flow is taken to be spatially uniform; such a flow is physically stable to any linear disturbance. Projecting the linearized Euler equations onto the random basis leads to a linear ROM, written here as

$$\dot{a}_j = A_{jk} a_k. \tag{50}$$

The ROM is stable if the maximum real part of the eigenvalues of the matrix A_{jk}, denoted $\lambda_{r_{max}}$, is less than or equal to zero. Fig. 1 plots $\lambda_{r_{max}}$ for ROMs consisting of one through eight basis functions. Using the symmetry inner product $(\cdot, \cdot)_H$ to construct the ROM results in a $\lambda_{r_{max}}$ of zero to machine precision. This is completely consistent with convection of a neutral disturbance in uniform flow and confirms that for any modal basis, this property of the linearized Euler equations is preserved by the ROM. For comparison, a second set of ROMs was constructed using the vector form of the unweighted L^2 inner product, Eq. (8), to project the equations. As seen in the figure, depending on the number of modes used in the ROM, the ROM can be stable or unstable. While this is a somewhat extreme case using "bad" modes, it is often the case that POD modes with small energy are largely comprised of numerical error and other high-frequency "noise." The symmetry inner product method ensures that such modes will not destabilize the ROM.

Fig. 1. Maximum real part of the eigenvalues of the ROM coefficient matrix A_{jk} for the case of random modes on a uniform base flow.
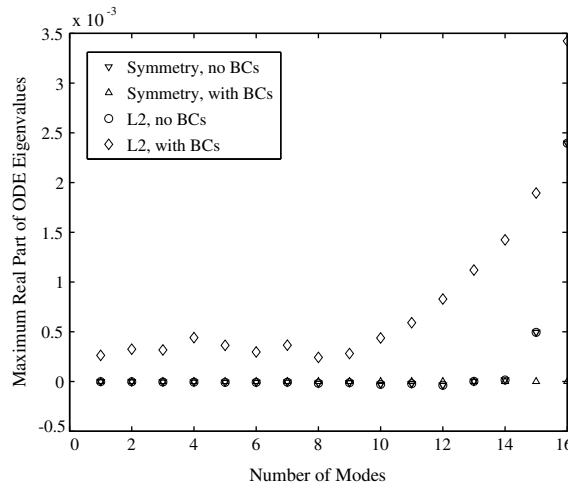
6.3. Test case: propagation of a one-dimensional acoustic pulse

A ROM is now constructed using CFD solutions of the following simple model problem. A one-dimensional acoustic pulse is prescribed as the initial condition,

$$u' = \exp(-(x - x_0)^2), \quad p' = \bar{\rho}\bar{c}u', \quad \frac{\rho'}{\bar{\rho}} = \left(\frac{p'}{\bar{p}}\right)^{\frac{1}{\gamma}} \quad v' = w' = 0, \qquad x_0 = 5 \tag{51}$$

The mean flow is taken as a uniform flow at Mach number $M = 0.5$. The pulse convects in the positive x direction at speed $\bar{u} + \bar{c}$, maintaining its shape. This problem was solved on a three-dimensional rectangular prism domain, with extent $0 \leqslant x \leqslant 20$, $-5 \leqslant y \leqslant 5$, $0 \leqslant z \leqslant 1$. The grid was composed of unstructured tetrahedral elements. Slip wall boundary conditions were applied on the constant y and z boundaries. The CFD simulation was performed over a nondimensional time $T_{tot} = 5.25$ with a total of 512 time steps. Snapshots were saved every eight simulation time steps and used to construct a 16 mode POD basis. Using the symmetry inner product, this basis captured essentially 100% of the snapshot energy (to six digits), while eight modes of this basis captured 99.5% and four modes captured 85.5%. The L^2 basis performed similarly in terms of energy capture of the snapshots.

Four different procedures were used to generate a fluid ROM for this problem: symmetry inner product with and without slip wall boundary conditions applied to the ROM and unweighted L^2 inner product with and without slip wall boundary conditions. The CFD code applies the slip wall condition only weakly, so that in general non-zero velocities were generated normal to the slip walls, resulting in non-zero boundary integrals in the ROM construction. Fig. 2 shows the maximum real part of the ROM eigenvalues for the different types of ROM. Only the symmetry inner product with boundary conditions

Fig. 2. Maximum real part of the eigenvalues of the ROM coefficient matrix A_{jk} for the 1-D pulse flow.

leads to a stable ROM. In this case, the computed maximum real part of the eigenvalues was less than 10^{-9}. The ROMs without boundary conditions are not stable, regardless of the inner product and the L^2 ROM with boundary conditions is the most unstable.

These results show that the symmetry formulation guarantees ROM stability, but only with the proper boundary conditions enforced. Note that the instabilities in all cases are very weak for this test case; accuracy of the ROMs over the solution time used to generate the ROM is comparable in each case. However, this is a relatively simple flow and stability properties in more complex flows may be less benign.
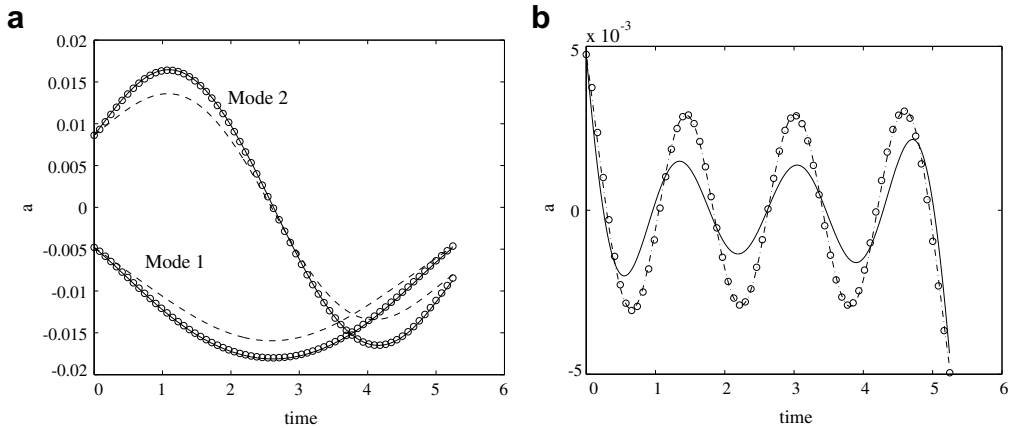
Fig. 3 shows the symmetry/with boundary conditions ROM solution for several modes, compared to the projection of the full CFD simulation onto the modes. The ROM results converge to the full simulation result as the number of modes increases.

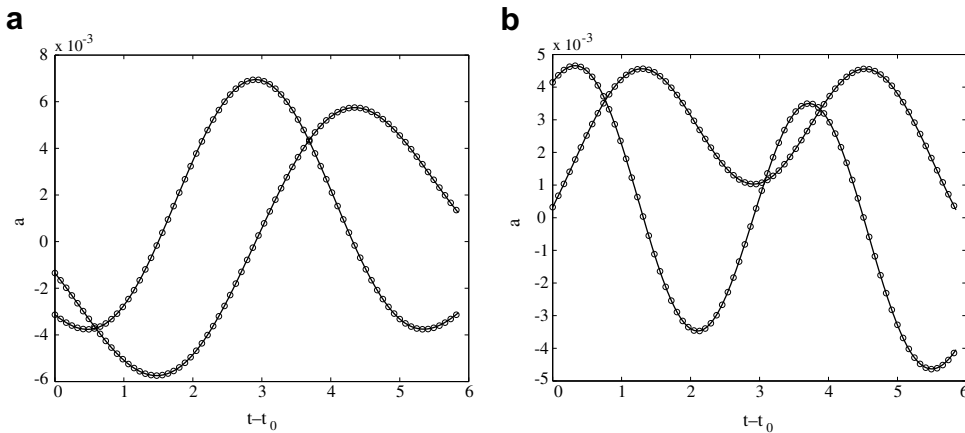### 6.4. Test case: reflection of a two-dimensional pressure pulse

A slightly more complicated situation is considered in this problem, where a two-dimensional pressure pulse reflects from walls of the domain. The mean flow is taken to be uniform with $M = 0.25$. The initial condition is taken as

$$p' = \exp(-((x - x_0)^2 + (y - y_0)^2)), \quad \frac{\rho'}{\bar{\rho}} = \left(\frac{p'}{\bar{p}}\right)^{\frac{1}{7}}, \quad u' = v' = w' = 0, \tag{52}$$
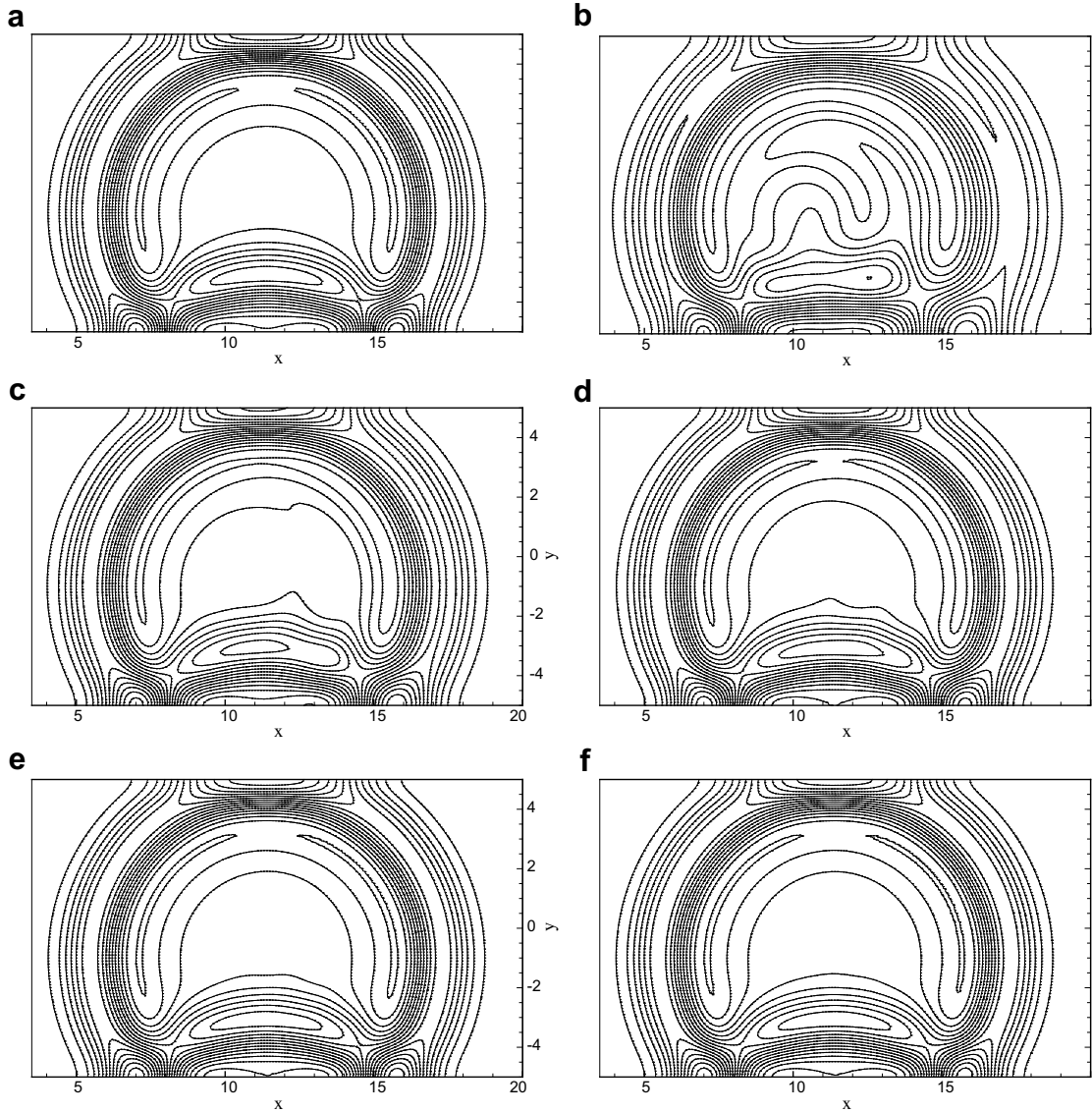
with $(x_0, y_0) = (10, -1)$. The same grid used in the previous section for the one-dimensional pulse is used here, with slip wall boundary conditions applied as before. The CFD simulation was run for a non-dimensional time of $T_{tot} = 6.4$ using 624 time

Fig. 3. Time history of modal amplitudes for acoustic pulse problem. ○, CFD simulation. – – –, 4 Mode ROM. —, 8 Mode ROM. – . – 12 Mode ROM. (a) Modes 1 and 2. (b) Mode 8.

Fig. 4. Time history of modal amplitudes for two-dimensional pressure pulse problem. ○, CFD simulation. —, 12 Mode ROM (a) Modes 1 and 2. (b) Modes 3 and 4.

Fig. 5. Pressure disturbance contours for the two-dimensional reflected pulse case, $t - t_0 = 5.0$. (a) CFD result. (b) 6 Mode ROM. (c) 8 Mode ROM. (d) 10 Mode ROM. (e) 12 Mode ROM. (f) 14 Mode ROM.

steps. Snapshots were saved every four time steps beginning at time $t = t_0 = 0.57$ and these were used to generate a 16-mode POD basis.

The symmetry inner product with boundary conditions applied again produced a stable ROM. Fig. 4 compares the projection of the CFD solution onto the first four modes (containing 85.6% of the snapshot energy) with the ROM prediction using 12 modes, demonstrating excellent agreement between the ROM and the CFD model. Fig. 5 compares the CFD pressure disturbance field with the field reconstructed from various ROM solutions at $t - t_0 = 5.0$. The reflection from the upper and lower walls is qualitatively captured by the ROM with only six modes. As the number of modes is increased the ROM result converges to the CFD solution, with no significant difference between the CFD solution and the 12 mode ROM solution.

A ROM for the two-dimensional pulse problem was also constructed using the L^2 inner product without a wall boundary condition. This ROM was only numerically stable when using six or seven modes; it was unstable for all other choices of basis size. However, due to the relatively small growth rate of the instability, accuracy over the length of the simulation was not compromised. Efficiency of the POD procedure was very similar for the symmetry and L^2 methods, with six modes capturing 97.4% of the snapshot energy for the symmetry case and 97.3% for the L^2 case. Accuracy of the ROM in recovering the CFD simulation was very similar between the two methods as well. These comparisons demonstrate that the symmetry method provides a guarantee of stability without sacrificing accuracy.

7. Conclusions

A method for computing reduced order models for linearized compressible flow has been developed and tested. The primary contribution of this new formulation is the introduction of a symmetry inner product for the linearized Euler equations which is guaranteed to produce stable ROMs. Accompanying boundary conditions have also been developed to preserve numerical stability for the case of the bounded domain.

The fluid ROM example problems presented show that the symmtery inner product formulation does indeed produce stable ROMs. However, in these examples the instabilities produced by the use of the L^2 inner product are only weak instabilities that do not have a practical effect on ROM accuracy. This is not to be expected in every case. For example, consider a time-periodic flow that one wishes to run for very long times. In such a flow, even weak instabilities can result in solution blow-up for long enough simulation times.

In future work we will consider application of stable Galerkin ROMs to more complicated flows and geometries, including flows with non-uniform base flow. We also plan to apply some of the mathematical principles used to develop symmetry inner products to the nonlinear Euler equations, in anticipation of an improved method for generating nonlinear ROMs.

Acknowledgments

Appendix. Far-field Boundary Conditions

The matrices that diagonalize $\mathbf{A}(\bar{\mathbf{q}}) \cdot \mathbf{n}$ according to Eq. (34) are

$$
S = \begin{pmatrix}
0 & n_3 & n_2 & \frac{1}{2}n_1 & -\frac{1}{2}n_1 \\
n_3 & 0 & -n_1 & \frac{1}{2}n_2 & -\frac{1}{2}n_2 \\
-n_2 & -n_1 & 0 & \frac{1}{2}n_3 & -\frac{1}{2}n_3 \\
n_1 & -n_2 & n_3 & -\frac{\bar{\zeta}}{2c} & -\frac{\bar{\zeta}}{2c} \\
0 & 0 & 0 & \frac{\gamma\bar{p}}{2c} & \frac{\gamma\bar{p}}{2c}
\end{pmatrix}
\tag{53}
$$

$$
S^{-1} = \begin{pmatrix}
0 & n_3 & -n_2 & n_1 & \frac{\bar{\zeta}n_1}{\gamma\bar{p}} \\
n_3 & 0 & -n_1 & -n_2 & -\frac{\bar{\zeta}n_2}{\gamma\bar{p}} \\
n_2 & -n_1 & 0 & n_3 & \frac{\bar{\zeta}n_3}{\gamma\bar{p}} \\
n_1 & n_2 & n_3 & 0 & \frac{c}{\gamma\bar{p}} \\
-n_1 & -n_2 & -n_3 & 0 & \frac{c}{\gamma\bar{p}}
\end{pmatrix}
\tag{54}
$$

$$
\Lambda = \begin{pmatrix}
\bar{u}_n & 0 & 0 & 0 & 0 \\
0 & \bar{u}_n & 0 & 0 & 0 \\
0 & 0 & \bar{u}_n & 0 & 0 \\
0 & 0 & 0 & \bar{u}_n + c & 0 \\
0 & 0 & 0 & 0 & \bar{u}_n - c
\end{pmatrix}
\tag{55}
$$

where $\bar{u}_n = \bar{\mathbf{u}} \cdot \mathbf{n}$. The vector of characteristic variables is then

$$
\mathbf{V}' \equiv S^{-1}\mathbf{q}' = \begin{pmatrix}
(n_3 v' - n_2 w' + n_1 \zeta') + \frac{\bar{\zeta}}{\gamma\bar{p}}n_1 p' \\
(n_3 u' - n_1 w' - n_2 \zeta') - \frac{\bar{\zeta}}{\gamma\bar{p}}n_2 p' \\
(n_2 u' - n_1 v' + n_3 \zeta') + \frac{\bar{\zeta}}{\gamma\bar{p}}n_3 p' \\
u'_n + \frac{c}{\gamma\bar{p}}p' \\
-u'_n + \frac{c}{\gamma\bar{p}}p'
\end{pmatrix}
\tag{56}
$$

In terms of the ROM basis $\boldsymbol{\phi}_k(\mathbf{x}) \equiv \left(\phi_k^1(\mathbf{x}) \quad \phi_k^2(\mathbf{x}) \quad \phi_k^3(\mathbf{x}) \quad \phi_k^4(\mathbf{x}) \quad \phi_k^5(\mathbf{x}) \right)^T, k = 1, \ldots, M$, the characteristic variables are

$$V' = \begin{pmatrix} \sum_{k=1}^{M}\left[n_1\left(\phi_k^4 + \left(\frac{\bar{z}}{c}\right)^2\phi_k^5\right) - n_2\phi_k^3 + n_3\phi_k^2\right]a_k(t) \\ \sum_{k=1}^{M}\left[-n_1\phi_k^3 - n_2\left(\phi_k^4 + \left(\frac{\bar{z}}{c}\right)^2\phi_k^5\right) + n_3\phi_k^1\right]a_k(t) \\ \sum_{k=1}^{M}\left[-n_1\phi_k^2 + n_2\phi_k^1 + n_3\left(\phi_k^4 + \left(\frac{\bar{z}}{c}\right)^2\phi_k^5\right)\right]a_k(t) \\ \sum_{k=1}^{M}\left[n_1\phi_k^1 + n_2\phi_k^2 + n_3\phi_k^3 + \frac{\bar{z}}{c}\phi_k^5\right]a_k(t) \\ \sum_{k=1}^{M}\left[-n_1\phi_k^1 - n_2\phi_k^2 - n_3\phi_k^3 + \frac{\bar{z}}{c}\phi_k^5\right]a_k(t) \end{pmatrix} \tag{57}$$

Recall that the farfield boundary integrand from Eq. (36) is $\phi_j^T H(\bar{\mathbf{q}})\mathbf{S}\Lambda\mathbf{V}_b'$. The portion $\phi_j^T H(\bar{\mathbf{q}})\mathbf{S}\Lambda$ is given by

$$\phi_j^T H(\bar{\mathbf{q}})\mathbf{S}\Lambda = \begin{pmatrix} \left[\bar{\rho}n_3\phi_j^2 - \bar{\rho}n_2\phi_j^3 + \alpha^2\bar{\rho}n_1\left(\gamma\bar{\rho}\bar{p}\phi_j^4 + \phi_j^5\right)\right]\bar{u}_n \\ \left[\bar{\rho}n_3\phi_j^1 - \bar{\rho}n_1\phi_j^3 - \alpha^2\bar{\rho}n_2\left(\gamma\bar{\rho}\bar{p}\phi_j^4 + \phi_j^5\right)\right]\bar{u}_n \\ \left[\bar{\rho}n_2\phi_j^1 - \bar{\rho}n_1\phi_j^2 + \alpha^2\bar{\rho}n_3\left(\gamma\bar{\rho}\bar{p}\phi_j^4 + \phi_j^5\right)\right]\bar{u}_n \\ \frac{1}{2}\left[\bar{\rho}n_1\phi_j^1 + \bar{\rho}n_2\phi_j^2 + \bar{\rho}n_3\phi_j^3 + \frac{1}{c}\phi_j^5\right](\bar{u}_n + c) \\ \frac{1}{2}\left[-\bar{\rho}n_1\phi_j^1 - \bar{\rho}n_2\phi_j^2 - \bar{\rho}n_3\phi_j^3 + \frac{1}{c}\phi_j^5\right](\bar{u}_n - c) \end{pmatrix}^T \equiv \begin{pmatrix} d_1(\mathbf{x}) \\ d_2(\mathbf{x}) \\ d_3(\mathbf{x}) \\ d_4(\mathbf{x}) \\ d_5(\mathbf{x}) \end{pmatrix}^T \tag{58}$$

Denote the boundary integral over the far-field boundary appearing in the jth ROM equation as I_{F_j}. The boundary conditions are implemented by altering, as required, the elements of the characteristic variable vector $\mathbf{V}_b'$ that correspond to incoming characteristics. The present treatment applies an approximately non-reflecting condition, that is the elements of $\mathbf{V}_b'$ corresponding to incoming characteristics are set to zero. Incoming characteristics are those with negative associated characteristic speed; the characteristic speeds are the diagonal entries of the matrix Λ. There are four possibilites:

Case 1: Supersonic Inflow ($\bar{u}_n < -c$)

Note that $\bar{u}_n < -c < 0 \Rightarrow \bar{u}_n - c < 0$ and $\bar{u}_n + c < 0$, i.e., all the characteristics are incoming. The approximate non-reflecting BC mandates that all incoming characteristics be set to zero. The far-field BC is thus

$$V_b' \equiv \mathbf{0} \in \mathbb{R}^5 \tag{59}$$

It follows that the far-field boundary integral I_{F_j} reduces to

$$I_{F_j} \equiv 0. \tag{60}$$

Case 2: Subsonic Inflow ($-c < \bar{u}_n < 0$)

Now, $\bar{u}_n < 0$, which implies $\bar{u}_n - c < 0$. However, $\bar{u}_n + c \in (0, c)$, in particular $\bar{u}_n + c > 0$. This means that the characteristics corresponding to the eigenvalues $\bar{u}_n$ and $\bar{u}_n - c$ are incoming whereas the characteristics corresponding to the eigenvalue $\bar{u}_n + c$ are outgoing. Looking at the definition of Λ in (55), we see that the characteristics to be set to zero correspond to the first, second, third and fifth component of V'. Thus, the far-field BC is

$$V_b' = \begin{pmatrix} 0 \\ 0 \\ 0 \\ \sum_{k=1}^{M}\left[n_1\phi_k^1 + n_2\phi_k^2 + n_3\phi_k^3 + \frac{\bar{z}}{c}\phi_k^5\right]a_k(t) \\ 0 \end{pmatrix} \tag{61}$$

It follows that the boundary integral component $I_{F_{jk}}$ reduces to

$$I_{F_j} = \sum_{k=1}^{M} a_k(t)\int_{\partial\Omega_F} d_4(\mathbf{x})\left[n_1\phi_k^1 + n_2\phi_k^2 + n_3\phi_k^3 + \frac{\bar{z}}{c}\phi_k^5\right]dS \tag{62}$$

Case 3: Subsonic Outflow ($0 < \bar{u}_n < c$)

In this case, $\bar{u}_n > 0$ implies that $\bar{u}_n + c > 0$ but $\bar{u}_n \in (0, c) \Rightarrow \bar{u}_n - c \in (-c, 0)$, i.e., $\bar{u}_n - c < 0$. This means that the characteristics corresponding to $\bar{u}_n - c$ are incoming whereas the characteristics corresponding to the other two eigenvalues are outgoing. It follows that the far-field BC to be implemented is

$$V'_b = \begin{pmatrix} \sum_{k=1}^{M} \left[n_1 \left(\phi_k^4 + \left(\frac{\bar{\zeta}}{c} \right)^2 \phi_k^5 \right) - n_2 \phi_k^3 + n_3 \phi_k^2 \right] a_k(t) \\ \sum_{k=1}^{M} \left[-n_1 \phi_k^3 - n_2 \left(\phi_k^4 + \left(\frac{\bar{\zeta}}{c} \right)^2 \phi_k^5 \right) + n_3 \phi_k^1 \right] a_k(t) \\ \sum_{k=1}^{M} \left[-n_1 \phi_k^2 + n_2 \phi_k^1 + n_3 \left(\phi_k^4 + \left(\frac{\bar{\zeta}}{c} \right)^2 \phi_k^5 \right) \right] a_k(t) \\ \sum_{k=1}^{M} \left[n_1 \phi_k^1 + n_2 \phi_k^2 + n_3 \phi_k^3 + \frac{\bar{\zeta}}{c} \phi_k^5 \right] a_k(t) \\ 0 \end{pmatrix} \tag{63}$$

and the desired boundary integral is

$$I_{F_j} = \sum_{k=1}^{M} a_k(t) \int_{\partial \Omega_F} \left\{ d_1(\mathbf{x}) \left[n_1 \left(\phi_k^4 + \left(\frac{\bar{\zeta}}{c} \right)^2 \phi_k^5 \right) - n_2 \phi_k^3 + n_3 \phi_k^2 \right] + d_2(\mathbf{x}) \left[-n_1 \phi_k^3 - n_2 \left(\phi_k^4 + \left(\frac{\bar{\zeta}}{c} \right)^2 \phi_k^5 \right) + n_3 \phi_k^1 \right] \right.$$
$$\left. + d_3(\mathbf{x}) \left[-n_1 \phi_k^2 + n_2 \phi_k^1 + n_3 \left(\phi_k^4 + \left(\frac{\bar{\zeta}}{c} \right)^2 \phi_k^5 \right) \right] + d_4(\mathbf{x}) \left[n_1 \phi_k^1 + n_2 \phi_k^2 + n_3 \phi_k^3 + \frac{\bar{\zeta}}{c} \phi_k^5 \right] \right\} dS \tag{64}$$

Case 4: Supersonic Outflow $(\bar{u}_n > c)$

Here, $\bar{u}_n > c \Rightarrow \bar{u}_n - c, \bar{u}_n + c > 0$, i.e., all the characteristics are outgoing. Hence the boundary integral is unaltered.

References

[1] L. Sirovich, Turbulence and the dynamics of coherent structures, part III: dynamics and scaling, Q. Appl. Math. 45 (3) (1987) 583–590.
[2] N. Aubry, P. Holmes, J. Lumley, E. Stone, The dynamics of coherent structures in the wall region of a turbulent boundary layer, J. Fluid Mech. 192 (1988) 115–173.
[3] P. Holmes, J.L. Lumley, G. Berkooz, Turbulence, Coherent Structures, Dynamical Systems and Symmetry, Cambridge University Press, 1996.
[4] K. Veroy, A.T. Patera, Certified real-time solution of the parametrized steady incompressible Navier–Stokes equations: rigorous reduced-basis *a posteriori* error bounds, Int. J. Num. Meth. Fluids 47 (2005) 773–788.
[5] K. Willcox, J. Peraire, Balanced model reduction via the proper orthogonal decomposition, AIAA J. 40 (11) (2002) 2323–2330.
[6] C.W. Rowley, Model reduction for fluids, using balanced proper orthogonal decomposition, Int. J. Bifurcat. Chaos 15 (3) (2005) 997–1013.
[7] T. Bui-Thanh, K. Willcox, O. Ghattas, B. van Bloemen Waanders, Goal-oriented, model-constrained optimization for reduction of large-scale systems, J. Comp. Phys. 224 (2007) 880–896.
[8] J.A. Taylor, M.N. Glauser, Towards practical flow sensing and control via POD and LSE based low-dimensional tools, J. Fluids Eng. 126 (3) (2003) 337–345.
[9] P.A. LeGresley, J.J. Alonso, Investigation of non-linear projection for POD based reduced order models for aerodynamics, AIAA Paper 2001-0926, 39th AIAA aerospace sciences meeting and exhibit, 2001.
[10] K.C. Hall, J.P. Thomas, E.H. Dowell, Proper orthogonal decomposition technique for transonic unsteady aerodynamic flows, AIAA J. 38 (10) (2000).
[11] T. Lieu, C. Farhat, M. Lesoinne, Reduced-order fluid/structure modeling of a complete aircraft configuration, Comput. Methods Appl. Mech. Eng. 195 (2006) 5730–5742.
[12] T. Lieu, C. Farhat, Aerodynamic parameter adaptation of CFD-based reduced-order models, AIAA Paper 2007-328, 45th aerospace sciences meeting and exhibit, 2007.
[13] Z. Bai, P.M. Dewilde, R.W. Freund, Reduced order modeling, in: W.H.A. Schilders, E.J.W. ter Maten (Eds.), Numerical Methods in Electromagnetics, Handbook of Numerical Analysis, vol. VIII, Elsevier, Amsterdam, 2005, pp. 825–895.
[14] F. Kwasniok, Empirical low-order models of barotropic flow, J. Atmos. Sci. 61 (2) (2004) 235–245.
[15] J.L. Lumley, Stochastic Tools in Turbulence, Academic Press, New York, 1971.
[16] C.W. Rowley, T. Colonius, R.M. Murray, Model reduction for compressible flows using POD and Galerkin projection, Physica D 189 (2004) 115–129.
[17] L. Sirovich, Chaotic dynamics of coherent structures, Physica D 37 (1989) 126–145.
[18] H.O. Kreiss, J. Lorenz, Initial-Boundary Value Problems and the Navier–Stokes Equations, Academic Press, Inc., 1989.
[19] D. Gottlieb, S.A. Orszag, Numerical analysis of spectral methods, SIAM, 1977.
[20] W.J. Layton, Stable Galerkin methods for hyperbolic systems, SIAM J. Numer. Anal. 20 (2) (1983) 221–233.
[21] B. Gustafsson, A. Sundström, Incompletely parabolic problems in fluid dynamics, SIAM J. Appl. Math. 35 (2) (1978) 343–357.
[22] T.J.R. Hughes, L.P. Franca, M. Mallet, A new finite element formulation for computational fluid dynamics: I. symmetric forms of the compressible Euler and Navier–Stokes equations and the second law of thermodynamics, Comput. Methods Appl. Mech. Eng. 54 (1986) 223–234.
[23] S.W. Bova, G.F. Carey, An entropy variable formulation and applications for the two-dimensional shallow water equations, Int. J. Num. Meth. Fluids 23 (1996) 29–46.
[24] B. Gustaffson, H.O. Kreiss, J. Oliger, Time Dependent Problems and Difference Methods, John Wiley & Sons, New York, NY, 1995.
[25] J. Oliger, A. Sundström, Theoretical and practical aspects of some initial boundary-value problems in fluid dynamics, SIAM J. Appl. Math. 35 (3) (1978) 419–446.
[26] S. Abarbanel, D. Gottlieb, Optimal time splitting for two- and three-dimensional Navier–Stokes equations with mixed derivatives, J. Comp. Phys 35 (1981) 1–33.
[27] B.-T. Chu, On the energy transfer to small disturbances in fluid flow (part I), Acta Mech. 1 (3) (1965) 215–234.
[28] C. Farhat, P. Geuzaine, G. Brown, Application of a three-field nonlinear fluid-structure formulation to the prediction of the aeroelastic parameters of an F-16 fighter, Comput. Fluids 32 (2003) 3–29.
[29] Michael A. Heroux, Roscoe A. Bartlett, Vicki E. Howle, Robert J. Hoekstra, Jonathan J. Hu, Tamara G. Kolda, Richard B. Lehoucq, Kevin R. Long, Roger P. Pawlowski, Eric T. Phipps, Andrew G. Salinger, Heidi K. Thornquist, Ray S. Tuminaro, James M. Willenbring, Alan Williams, Kendall S. Stanley, An overview of the trilinos project, ACM Trans. Math. Softw. 31 (3) (2005).
[30] B. Kirk, J.W. Peterson, R.H. Stogner, G.F. Carey, `libMesh`: A C++ library for parallel adaptive mesh refinement/coarsening simulations, Eng. Comput. 22 (3–4) (2006) 237–254.